LNF-96/034(P)

Alignment Procedure for the VIRGO Interferometer: Experimental Results from the Frascati Prototype

D. Babusci, H. Fang, G. Giordano, G. Matone, L. Matone, V. Sannibale

Physics Letters A 226, 31-40, (1997)

ELSEVIER

10 February 1997

Physics Letters A 226 (1997) 31–40

PHYSICS LETTERS A

Alignment procedure for the VIRGO interferometer: experimental results from the Frascati prototype

D. Babusci [1], H. Fang, G. Giordano, G. Matone, L. Matone, V. Sannibale [2]

INFN – Laboratori Nazionali di Frascati, P.O. Box 13, I-00044 Frascati, Italy

Received 3 September 1996; revised manuscript received 8 November 1996; accepted for publication 27 November 1996
Communicated by P.R. Holland

Abstract

A small fixed-mirror Michelson interferometer has been built in Frascati to experimentally study the alignment method that has been suggested for VIRGO. The experimental results fully confirm the adequacy of the method. The minimum angular misalignment that can be detected in the present setup is 10 nrad/$\sqrt{\text{Hz}}$.

PACS: 07.60.Ly; 04.80.+z

1. Introduction

The search for gravitational waves (GW) with interferometric antennas (VIRGO, LIGO, GEO) aims at the detection of a GW signal by measuring the relative motion that a GW induces between two widely separated test masses [1–3]. In all these antennas, the test masses are the mirrors suspended at the ends of two long arms, perpendicular to each other and forming a Michelson interferometer, with Fabry–Perot cavities in the VIRGO and LIGO cases. Inside the detector, IR-light (1.064 μm) is split into two beams which travel down the arms and reflect from the mirrors at the two ends. On their return, the beams interfere on the detection plane and from the illumination changes of the photodiode one can infer the relative changes that have occurred to the interferometer arm lengths. However, all the optical elements of the interferometer undergo position and angle fluctuations that are mostly due to thermal and seismic noise. Any angular tilt leads to a reduction in the sensitivity of the interferometer and in particular causes a variation of the cavity length that simulates a GW signal.

The specifications required for the angular stability are determined by the sensitivity level one is aiming at for the detection of a GW signal. These can turn out to be very severe and thus the sensitivities required in monitoring the error signals can become an issue. As a part of the research and development program in support of the VIRGO project, we built a small fixed-mirror interferometer with Fabry–Perot cavities in the two arms. The aim of the work was only to focus on the experimental verification of the theory developed to compute the alignment signals and on the method to extract from them the angular position of each individual mirror.

[1] E-mail: babusci@ibmllv.lnf.infn.it.

[2] Present address: L.A.P.P., Chemin de Bellevue, BP 110, 74941 Annecy-le-Vieux Cedex, France.

PII S0375-9601(96)00907-3

2. The Fabry–Perot alignment methods

We considered two basic alignment methods, both of them based on the phase modulation of the incoming beam. The first was developed at Caltech by Anderson et al. [4] and the second at Glasgow by Ward et al. [5]. Both of them were originally designed to align one single Fabry–Perot (FP) but no attempt has ever been made to extend this procedure to the case of a complete Michelson interferometer (MI).

For a brief description of the two methods, let us consider a pure TEM_{00} laser beam entering a Fabry–Perot cavity with a tilting angle $\Delta\alpha$ with respect to the cavity axis. In the limit where this angle is much smaller than the far field divergence of the beam $\alpha_0 = \lambda/\pi w_0$, the cavity sees the input beam as a linear superposition of the TEM_{00} distribution and the first off-axis mode TEM_{10}. Similarly, if the TEM_{00} beam enters the cavity with a lateral displacement Δx much smaller than the beam waist w_0, the cavity sees again the incoming beam profile as a linear superposition of TEM_{00} and TEM_{10}.

The difference between these two cases is that the rotations lead to a coupling into the TEM_{10} mode as the translations do, but with a 90° phase shift. This means that a misalignment causes a coupling into the lowest-order off-axis mode with a phase that depends upon the type of misalignment. Therefore the transverse field distribution, seen by the cavity as a consequence of small walks off the two terminal mirrors, can be always approximated by a linear combination of these two cavity modes,

$$E \simeq C_0(U_0 + CU_1)\,, \tag{2.1}$$

where E is the normalized input field, and U_0 and U_1 are the usual orthonormal Hermite-Gaussian functions of x, y associated with the TEM_{00} and TEM_{10} modes. C_0 and C are the coupling coefficients and in particular

– for a pure translation Δx: $C = \Delta x/w_0$;

– for a pure rotation $\Delta\alpha$: $C = \mathrm{i}\Delta\alpha/\alpha_0$;

C_0 is always real and, since it is always very close to unity, it has been assumed equal to one.

Therefore, the basic idea of the methods is to find a way to detect the amplitude and phase of this induced TEM_{10} component.

2.1. The Anderson method

With this method, one chooses to phase modulate the input beam at the frequency separation between TEM_{00} and TEM_{10}, which in a plano-concave cavity (length L, mirror radius R) is given by

$$\Delta\nu = \frac{c}{2\pi L}\arccos\sqrt{1 - L/R}\,. \tag{2.2}$$

The field amplitude for a beam of phase-modulated light at the optical frequency ω has the form

$$E = E_0 \mathrm{e}^{\mathrm{i}\omega t}\Bigg(J_0(m) + \sum_{l=1}^{l=\infty} J_l(m)\,[\mathrm{e}^{\mathrm{i}l\Omega t} + (-1)^l \mathrm{e}^{-\mathrm{i}l\Omega t}]\Bigg)\,, \tag{2.3}$$

where $\Omega/2\pi = \Delta\nu$ is the modulation frequency, E_0 is a constant real vector, and $J_l(m)$ is the Bessel function of order l and phase modulation index m. In this notation, the physical electric field is obtained by taking the real part of the complex quantities. If the value of the modulation index m is sufficiently small, only the first three terms in the expansion (2.3) can be retained and the expression of the electric field (2.1) reduces to

$$E \simeq E_0(U_0 + CU_1)\mathrm{e}^{\mathrm{i}\omega t}[\,J_0(m) + 2\mathrm{i}J_1(m)\sin\Omega t\,]\,. \tag{2.4}$$

By retaining only the resonant terms, namely the fundamental mode at the carrier frequency and the TEM_{10} mode at the sideband frequency $(\omega + \Omega)$, the resulting transmitted intensity exhibits a spatially dependent component modulated at the beat frequency Ω as follows ($I_0 = |\,E_0\,|^2$),

$$I = |\,\mathcal{T}^2\,|\,I_0\{J_0^2U_0^2 + |\,C\,|^2\,J_1^2U_1^2 + 2J_0J_1U_0U_1(\,\mathrm{Re}[C]\cos\Omega t + \mathrm{Im}[C]\sin\Omega t)\}\,, \tag{2.5}$$

where $\mathcal{T}$ is the FP's complex transmittivity on resonance [7].

Since the Hermite–Gaussian functions are mutually orthogonal when integrated all over the space, the detection of the entire transmitted beam by a single photodiode results in a DC signal. The correspondent DC

photocurrent is obtained by integrating the first and leading term of Eq. (2.5), obtaining

$$I_{\mathrm{dc}} = \eta \frac{e\lambda}{hc} \mid \mathcal{T} \mid^2 I_0 J_0^2(m) \,, \tag{2.6}$$

where η is the quantum efficiency. On the contrary, a separate detection of each half of the transmitted beam, followed by electronic subtraction of the two photocurrents, yields a current signal given by

$$I_{\mathrm{diff}} = 2\sqrt{\frac{2}{\pi}}\, I_{\mathrm{dc}} \frac{J_1}{J_0} (\,\mathrm{Re}[C]\cos\Omega t + \mathrm{Im}[C]\sin\Omega t) \,. \tag{2.7}$$

This equation shows that the intensity component that is in-phase with the modulation ($\cos\Omega t$) is proportional to the translational error and the in-quadrature component ($\sin\Omega t$) is proportional to the angular alignment error. Thus, by demodulating the signal, one can obtain simultaneously and independently both the misalignment errors. With the same argument, a quadrant photodiode detector permits simultaneous detection of couplings to both vertical and horizontal off-axis modes.

2.2. The Ward method

This alternative technique was suggested by Drever at Caltech and experimentally demonstrated by Ward at the University of Glasgow [5]. It is basically an extension of the method used for the longitudinal locking (Pound and Drever) [6] and it uses the light which is reflected from the FP. The beam is phase modulated but the modulation frequency Ω is not to be equal to the frequency difference between fundamental and first transverse mode as it is in the Anderson method.

Let us suppose that a plano-concave cavity is both laterally and angularly misaligned with respect to the incoming beam direction of the usual quantities $a = \Delta x/w_0$ and $\alpha = \Delta\alpha/\alpha_0$, respectively, with Δx being measured at the waist position. In the cavity frame the incoming beam is described by

$$E'_{\mathrm{in}} = E_0 \mathrm{e}^{\mathrm{i}\omega t}[\,U_0 + (a + \mathrm{i}\alpha)U_1\,][\,J_0 + 2\mathrm{i}J_1 \sin\Omega t\,] \,, \tag{2.8}$$

where U_0 at the carrier frequency is the only resonant term, and all the other terms are assumed to be completely off-resonance. With the convention that the reflection from a mirror introduces a 90° phase shift, the phase of a beam reflected from a Fabry–Perot is $-90°$ ($+90°$) depending on whether the beam is on (off) resonance. Assuming a totally reflective end mirror, the expression for the reflected beam in the cavity frame is

$$E'_{\mathrm{ref}} = -\mathrm{i}E_0 \mathrm{e}^{\mathrm{i}\omega t}\{J_0[\,U_0 - (a + \mathrm{i}\alpha)U_1\,] - 2\mathrm{i}J_1[\,U_0 + (a + \mathrm{i}\alpha)U_1\,]\sin\Omega t\} \,, \tag{2.9}$$

which, transformed into the incoming beam frame, reads as follows,

$$E_{\mathrm{ref}} = -\mathrm{i}E_0 \mathrm{e}^{\mathrm{i}\omega t}[\,J_0(U_0 - 2aU_1) - 2\mathrm{i}J_1(U_0 + 2\mathrm{i}\alpha U_1)\sin\Omega t\,] \,. \tag{2.10}$$

The idea of the method is to let this beam evolve freely in space and to consider that an additional term intervenes in this process. This term is the phase difference between the real Hermite–Gaussian beam and an ideal plane wave, given by the Guoy phase

$$\phi_{n,m}(z) = (n + m + 1)\phi(z) \,, \qquad \tan\phi(z) = \frac{\lambda z}{\pi w_0^2} \,. \tag{2.11}$$

The indexes n, m refer to the (n, m)th order mode and z is the propagation coordinate whose origin, $z = 0$, is at the location of the beam waist. This means that different modes evolve differently and the two components U_0 and U_1 acquire the phase difference $\phi(z)$. Eq. (2.10) becomes

$$E_{\mathrm{ref}}(z) = -\mathrm{i}E_0 \mathrm{e}^{\mathrm{i}(\omega t + \phi)} \times \{[\,J_0(U_0 - 2aU_1\cos\phi) - 4\alpha J_1\cos\phi\sin\Omega t] - 2\mathrm{i}[\,aJ_0U_1\sin\phi + J_1(U_0 - 2\alpha U_1\sin\phi)\sin\Omega t]\} \,. \tag{2.12}$$

The intensity associated with this field depends upon the position where the detector is located. If the current difference between the two halves of a photodetector is taken at a given z-position, and the signal is demodulated at the frequency Ω, the dominant component that will be detected is given by

$$I_{\mathrm{diff}} \propto -J_0 J_1 U_0 U_1 (a\sin\phi + \alpha\cos\phi)\sin\Omega t \,. \tag{2.13}$$

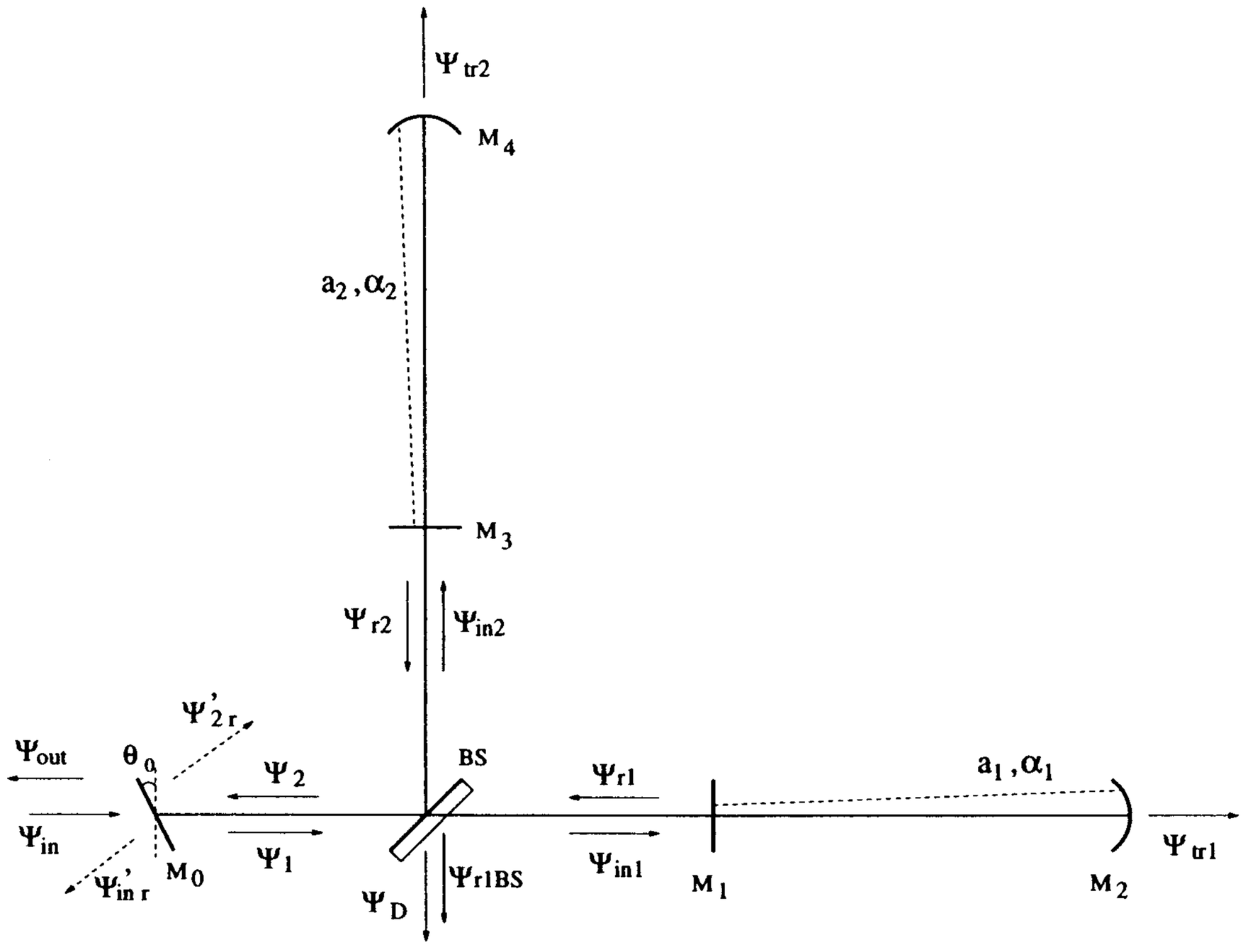

Fig. 1. Beams in a misaligned interferometer

Since the beam has a waist on M_1, $\sin\phi = 0$ right behind M_1 and in this region the method is sensitive only to tilts. However, if the beam is let to evolve, the angle ϕ goes to $\pi/2$ and so, at a very large distance from the waist, I_{diff} becomes sensitive only to displacements. A more practical way to change ϕ is to employ an appropriate telescope, as discussed in detail in Ref. [5].

3. Beam evolution inside a complex interferometer

Let us consider a TEM_{00} phase-modulated beam Ψ_{in},

$$\Psi_{\mathrm{in}} = U_0 e^{i\omega t}(J_0 + 2iJ_1 \sin \Omega t)\,, \qquad (3.1)$$

impinging on a misaligned interferometer of a VIRGO-like structure (see Fig. 1) with the beam waist on M_0. In the following the "main frame" will always refer to this input beam.

In order to compute the expected alignment signals, we have developed a mathematical procedure that, under the following approximations and assumptions, leads to a fully analytical solution,

(1) the beam mismatches, due to the difference in length of the Michelson arms, and to the plane–plane configuration of the recycling cavity (VIRGO case), have been neglected;

(2) all the misalignment angles are assumed to be much smaller than the angular divergence of the beam;

(3) second or higher order terms in the misalignment angles have been neglected in the expressions of the beam amplitudes;

(4) since, under the above approximations, no horizontal–vertical coupling can be envisaged, the analysis has been limited to one plane only;

(5) since in Virgo the angular noises that need to be corrected are confined in the region below 1 Hz, the calculation has been performed in a static condition, i.e. with all the optical elements being kept at their misaligned positions.

Under the above conditions, all the beams running along or emerging from the interferometer can be expressed as a linear combination of TEM_{00} and TEM_{10}.

Hence, each frequency component of the beam Ψ_1 (see Fig. 1) can be written in the following form,

$$\Psi_1 = A\mathrm{e}^{\mathrm{i}\theta}[U_0 + (a + \mathrm{i}\alpha)U_1], \tag{3.2}$$

where A, θ, a, α are the four quantities to be determined. Once this expression is given, all the other beams follow immediately, since the distances between the optical elements and the propagation phases are all known. After the beam Ψ_1 has been transported to the two FPs, the reflected beams Ψ_{r1} and Ψ_{r2} are calculated according to a procedure similar to the one of Section 2.2. These two reflected beams are then propagated back toward the beam splitter and their recombination Ψ_2 hits the recycling mirror M_0 which is supposed to be misaligned of the angle θ_0. The expression for the reflected beam in the main frame takes the form

$$\Psi_{2r} = A^*\mathrm{e}^{\mathrm{i}\theta^*}[U_0 + (a^* + \mathrm{i}\alpha^*)U_1], \tag{3.3}$$

where the quantities $A^*, \theta^*, a^*, \alpha^*$ contain A, θ, a, α, the propagation phases, and the angles of all the mirrors. Finally, by imposing that the sum $\Psi_{2r} + t_0\Psi_{\mathrm{in}} = \Psi_1$, one obtains

$$\begin{aligned} &t_0U_0J_i + A^*\mathrm{e}^{\mathrm{i}\theta^*}[U_0 + (a^* + \mathrm{i}\alpha^*)U_1] \\ &\quad = A\mathrm{e}^{\mathrm{i}\theta}[U_0 + (a + \mathrm{i}\alpha)U_1]. \end{aligned} \tag{3.4}$$

By equalizing real and imaginary parts of U_0, U_1, Eq. (3.4) can be broken down into a system of four linear equations in the four unknowns A, θ, a, α. The solution of this system shows that A and θ do not depend on the misalignment angles, while a and α are given by

$$a = \sum_{j=0}^{4} b_j\theta_j, \quad \alpha = \sum_{j=0}^{4} c_j\theta_j, \tag{3.5}$$

where the b_i, c_i coefficients depend on the geometrical and optical characteristics of the interferometer (propagation phases, mirrors transmittivities and reflectivities).

Once this procedure has been repeated for all the three frequency components, we have the full description of the beam inside the recycling cavity that can be propagated toward any position of interest, inside or outside the interferometer. Given a quadrant photodiode placed on an output beam, four signals can be detected: up–down and left–right differences demodulated in-phase and in-quadrature. In general, a signal S^i from the ith quadrant photodiode will be of the form

$$S^i = \sum_{k=0}^{4} C_k^i\theta_k. \tag{3.6}$$

This means that each signal will receive contributions from any misalignment and one has to find a way to extract the information relative to each of the five mirrors. The most common way of solving a problem of this kind is the χ^2 procedure: having n signals (with $n \geqslant 5$), the best estimate of the angles θ_j is found searching for the set of values leading to the minimum χ^2. In this case, given the simple structure of Eq. (3.6), this set of θ_j-values can be obtained analytically, together with their uncertainties $\Delta\theta_j$, due to the presence of noise on the signals (shot-noise and electronic noise).

The reconstruction of the mirror angles can be optimized by choosing a sufficient number of quadrant photodiodes and by studying the dependence of their signal on the Guoy phase.

4. The experimental apparatus

The Frascati prototype is a small-scale, fixed-mirror Michelson interferometer in air, sufficient for us to concentrate on optical alignment and stability studies. The mechanical and optical apparatus lies on top of a TMC-optical table (1.5 m × 2.0 m), which is isolated from seismic ground motion with an air overpressure spring system that couples it to the ground floor. A sound absorbing enclosure protects the whole assembly against the ambient acoustical noise. The interferometer is constructed with commercial mirror mounts and the space between the cavity mirrors is protected by plexiglass tubes to minimize the fluctuations in the refraction index induced by air circulation.

4.1. The interferometer layout

The layout is shown in Fig. 2. Light from a frequency stabilized Newport NL-1 He-Ne laser (0.5 mW at 632.8 nm) is phase modulated and focused with two positive lenses (L_0, L_1) into a beam

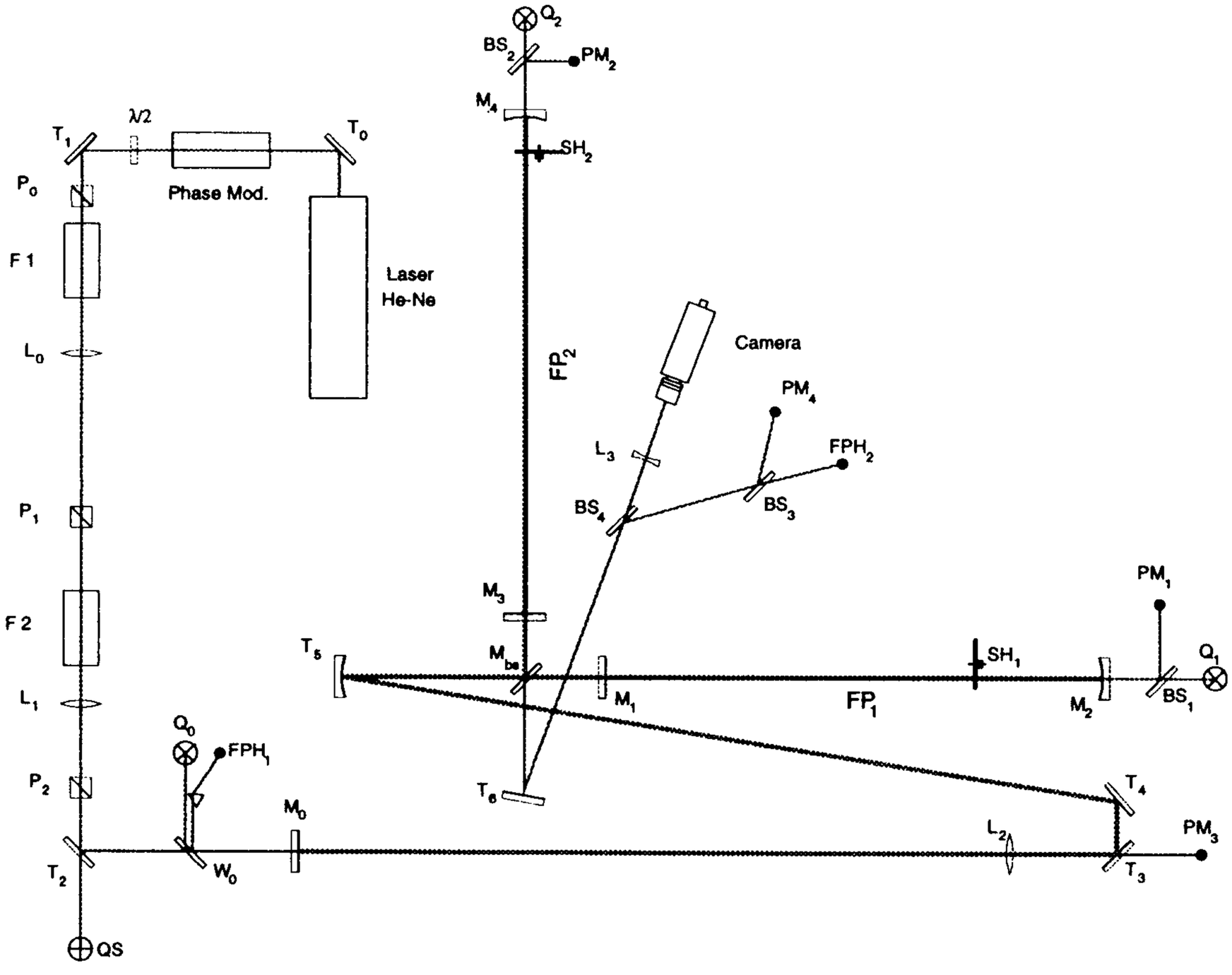

Fig. 2. Complete lay-out of the whole interferometer

waist of 5.9×10^{-2} cm at the position of the recycling mirror (M_0), 1.94 m away from the laser output.

The laser is isolated from spurious light feedbacks with a system of two Faraday rotators and two polarizing beam splitters. If only one of these two systems is used, the back reflection reduces to a fraction of 2.0×10^{-5} of the incident power but becomes undetectable with a cascade of two. A third polarizing beam splitter (P_2) is added before the entrance of the interferometer to ensure linear polarization in the horizontal plane for both the beams directed to and reflected from the interferometer. A quadrant photodiode (QS) is placed on the beam transmitted from the mirror T_2: low frequency movements of the beam directed to the interferometer, due mainly to angular jitters of the laser output, are so detected and corrected, acting in a feedback loop on two piezos mounted on the mirror T_0.

To find room on the optical table, the recycling cavity is folded over a zig-zag sequence of two flat mirrors (T_3, T_4), a positive lens (L_2) and a curved mirror

Table 1
Mirrir characteristics

Mirror	Transmittivity t^2 (%)	Curvature radius (m)
M_0	40.8 ± 0.3	∞
M_1, M_3	10.1 ± 0.2	∞
M_2, M_4	0.2 ± 0.01	10
BS	50.3 ± 0.7	∞
T_3	$(6.0 \pm 1.0) \times \times 10^{-2}$	∞

(T_5) with a total optical path of 2.68 m. The beam waist at the position of the two flat mirrors (M_1, M_3) is 7.2×10^{-2} cm and is mode-matched to the geometry of the two following FP cavities. The FP mirrors ($M_{1,2}$ and $M_{3,4}$) and the recycling mirror (M_0) are mounted on Burleigh PZ-91 (piezo-mounting) to allow for fine longitudinal (2 nm/V) and angular adjustments (80 nrad/V horizontal, 92 nrad/V vertical). The mirror characteristics have been measured and the results are summarized in Table 1.

The piezo mounts have a frequency response that

relates the applied voltage to the motion effectively executed by the mirror. This response is described by a transfer function which, in general, depends upon the exciting frequency and can only be determined with an experimental measurement. In the low frequency interval ($\leqslant$ 10 Hz), where most of the mechanical noise is concentrated, the transfer function is definitely well-behaved. However, structures are visible in the region between 200 Hz and 500 Hz and are associated with the mechanical structure of the mirror holder. They have been efficiently damped by adding an extra load to the mount.

4.2. Fabry–Perot cavities

Both the Fabry–Perot cavities are 70.6 cm long and the separation between the longitudinal modes is $c/2L = 212.3$ MHz. From Eq. (2.2), the transverse-longitudinal separation is 18.2 MHz. The line-shape profile has been measured with a photodiode located behind the terminal mirrors and reproduces the expected expression in Ref. [7]. The measurement of the width Γ of the resonance yields the finesse

$$\mathcal{F} = \frac{c}{2L\Gamma} = \pi\frac{\sqrt{r_1 r_2}}{1 - r_1 r_2} = 57.5 \pm 2.0 \qquad (4.1)$$

and allows for a direct measurement of the product $r_1 r_2 = 0.947 \pm 0.002$, in good accordance with the reflectivity values reported in Table 1. The value of the power enhancement (the power stored into the cavity per unit incident power), the reflectivities and the transmittivities of the FPs have been measured at resonance and the results are shown in Table 2 together with the same values expected on the base of the mirror transmittivities quoted in Table 1. The departure from one of the sum $T^2 + R^2$ measures the total amount of the cavity losses. They turn out to be 7.5% and 9.4% for FP_1 and FP_2 and imply coating losses of 0.11% and 0.15%, both well within specs for standard commercial mirrors.

Both FP cavities have been longitudinally locked with a "dithering" technique. The end mirrors of FP1 and FP2 are set into longitudinal oscillation with an amplitude of $\sim 1.3 \times 10^{-5}\lambda$ at a frequency of 7.0 kHz and 4.3 kHz, respectively. By means of two analog dividers, the detectors $PM_{1,2}$ have been normalized to PM_3 which is proportional to the recycling cavity inner power. The resulting ratios are then sent to two lock-in amplifiers, with reference 7.0 kHz and 4.3 kHz, whose outputs constitute the error signals of the feedback loops. These signals are then integrated, amplified and, finally, applied to the piezos of the two FPs' terminal mirrors M_2 and M_4. In the "feedback on" condition, the power fluctuations in the two cavities never exceed a small percentage of the stored power.

Table 2
Reflectivities and the transmittivities of the FPs

	Reflectivity R^2 (%)	Transmittivity T^2 (%)	Power enhancement
FP_1	85.8 ± 3.0	6.7 ± 0.2	32.8 ± 1.0
FP_2	84.3 ± 3.0	6.3 ± 0.2	31.1 ± 1.0
expected	92.6	7.4	36.2

4.3. The recycling cavity

The recycling cavity comprises the sequence of elements that run from M_0 to $M_{1,3}$. It is arranged in a plano–plano geometry where the two flat terminal mirrors are connected by the two focusing elements L_2 and T_5. The distances from the beam splitter to the initial FP mirrors have been made slightly different ($M_{BS} - M_1 = 11.9$ cm, $M_{BS} - M_3 = 9.4$ cm), in analogy to what they will be in VIRGO, to increase the signal on the dark fringe detector [8]. The total cavity loss α_{rc}, inclusive of the lens L_2 and the three mirrors T_3, T_4, T_5, has been obtained by a direct measurement of the power lost in one trip from L_2 to T_5. Unfortunately measurements of this kind are affected by large errors because they always require to take differences between almost equal numbers. In our case we have obtained $\alpha_{rc} = (1.92 \pm 1.0)\%$.

The recycling cavity can be looked at as a FP cavity where the initial mirror is M_0 and the terminal mirror is the ensemble of the beam splitter and the two FPs. This ensemble can be considered as an equivalent mirror with an effective reflectivity defined as

$$r_{eq}^2 = \tfrac{1}{2}(R_{FP_1}^2 + R_{FP_2}^2)(1 - \alpha_{rc})^2(1 - \alpha_{fr}) = (81.5 \pm 2.6)\%, \qquad (4.2)$$

where α_{fr} accounts for the power that is inevitably lost in the incomplete light extinction on the fringe detector. This power loss has been evaluated to be

Table 3
Beam reflected from M_0 for a fixed value of Φ_G/π: comparison between the experimental and theoretical values for the quantity $R_{ij} = A(M_i)/A(M_j)$ and $\Delta\varphi_{ij} = |\varphi(M_i) - \varphi(M_j)|$

$\Phi_G/\pi = 0.1063$	R_{12}	$\Delta\varphi_{12}$ (deg)	R_{20}	$\Delta\varphi_{20}$ (deg)	R_{30}	$\Delta\varphi_{30}$ (deg)
experiment	1.45 ± 0.08	174.3 ± 3.0	1.33 ± 0.06	1.2 ± 1.6	1.33 ± 0.07	179.3 ± 3.1
theory	1.22	179.0	1.26	1.1	1.11	179.1

Table 4
Beam transmitted from FP_1

$\Phi_G/\pi = 0.0415$	R_{02}	$\Delta\varphi_{02}$ (deg)	R_{12}	$\Delta\varphi_{12}$ (deg)	R_{42}	$\Delta\varphi_{42}$ (deg)
experiment	0.40 ± 0.02	45.1 ± 3.0	0.83 ± 0.03	173.8 ± 2.2	0.8 ± 0.1	25.2 ± 6.5
theory	0.395	49.6	0.835	174.7	0.7	23.0

of the order of 1%. The enhancement factor for this cavity is expected to be

$$F_{\mathrm{pe}} = \frac{\text{stored power}}{\text{incident power}} = \frac{T_0^2}{(1 - r_{\mathrm{eq}} r_0)^2} = 4.4 \pm 0.4 \tag{4.3}$$

and it has been obtained by measuring the power transmitted from T_3 (or equivalently by $FP_{1,2}$) with and without the insertion of M_0. The experimental result has been determined to be 4.8 ± 0.3, in good agreement with Eq. (4.3).

Two fast photodiodes were used in two feedback loops to keep the recycling cavity on resonance (FPH_1) and to maintain the dark fringe condition (FPH_2). The demodulated signal from FPH_1 was used to control the M_0 position, while the feedback from FPH_2 acted on both the FP_2 mirrors, thus constraining the dark fringe without perturbing the status of FP_2.

5. Experimental results

According to the analytical simulation described in Section 3 (for more details see Ref. [9]), small mirror misalignments do not prevent the field amplitude from reaching an equilibrium condition that retains the information on each individual mirror position. This means that the demodulated signals from a quadrant photodiode placed on any of the beams leaving the interferometer are sensitive to the misalignment status of all mirrors, either in their in-phase or in-quadrature components, or in both. Furthermore, since each of these components can be analytically expressed in terms of the individual mirror misalignments, with a sufficient number of measurements the alignment status of the whole interferometer can be fully determined. To better achieve this, the modulation frequency of the laser beam has to coincide with the TEM_{00}–TEM_{10} frequency separation of the FPs (18.2 MHz in our case), since in this way the beams transmitted from the FPs have the maximum sensitivity to misalignments.

In the experimental test we conducted, we set into oscillation M_0, M_1, M_2, M_3, M_4 one at a time, at the fixed frequency of 3 Hz and with an amplitude of approximately 200 nrad. The signals seen by Q_0, Q_1 and Q_2 were each time demodulated at 0° and 90° in order to construct the two quantities

$$A(M_i) = \sqrt{I^2(M_i) + Q^2(M_i)}\,,$$
$$\varphi(M_i) = \arctan \frac{I(M_i)}{Q(M_i)}\,. \tag{5.1}$$

where $I(M_i)$ and $Q(M_i)$ are the in-phase and in-quadrature signals generated by the ith mirror.

Since the angle/voltage calibrations are the same for all the piezos in the system, it is quite appropriate to present the results normalized to one of them. Tables 3–5 present the comparison between the experimental and expected values of these ratios for Q_0, Q_1 and Q_2, respectively.

As shown in the tables, we have selected different values for the Guoy phases, either by choosing the appropriate position of the quadrant photodiode, or by

Table 5
Beam transmitted from FP_2 for two values of Φ_G/π

	$\Phi_G/\pi = 0.0965$		$\Phi_G/\pi = 0.4144$	
	experiment	theory	experiment	theory
R_{02}	0.52 ± 0.02	0.57	0.56 ± 0.01	0.55
$\Delta\varphi_{02}$ (deg)	10.1 ± 2.0	26.7	15.5 ± 1.4	24.2
R_{12}	0.77 ± 0.02	0.91	0.9 ± 0.02	0.895
$\Delta\varphi_{12}$ (deg)	183.8 ± 1.4	179.2	176.7 ± 1.0	179.2
R_{32}	1.28 ± 0.03	1.2	0.94 ± 0.02	1.17
$\Delta\varphi_{32}$ (deg)	146.6 ± 1.27	152.4	137.6 ± 1.0	149.2
R_{42}	1.2 ± 0.03	1.43	1.18 ± 0.01	1.39
$\Delta\varphi_{42}$ (deg)	31.9 ± 1.1	22.4	35.3 ± 0.6	24.6

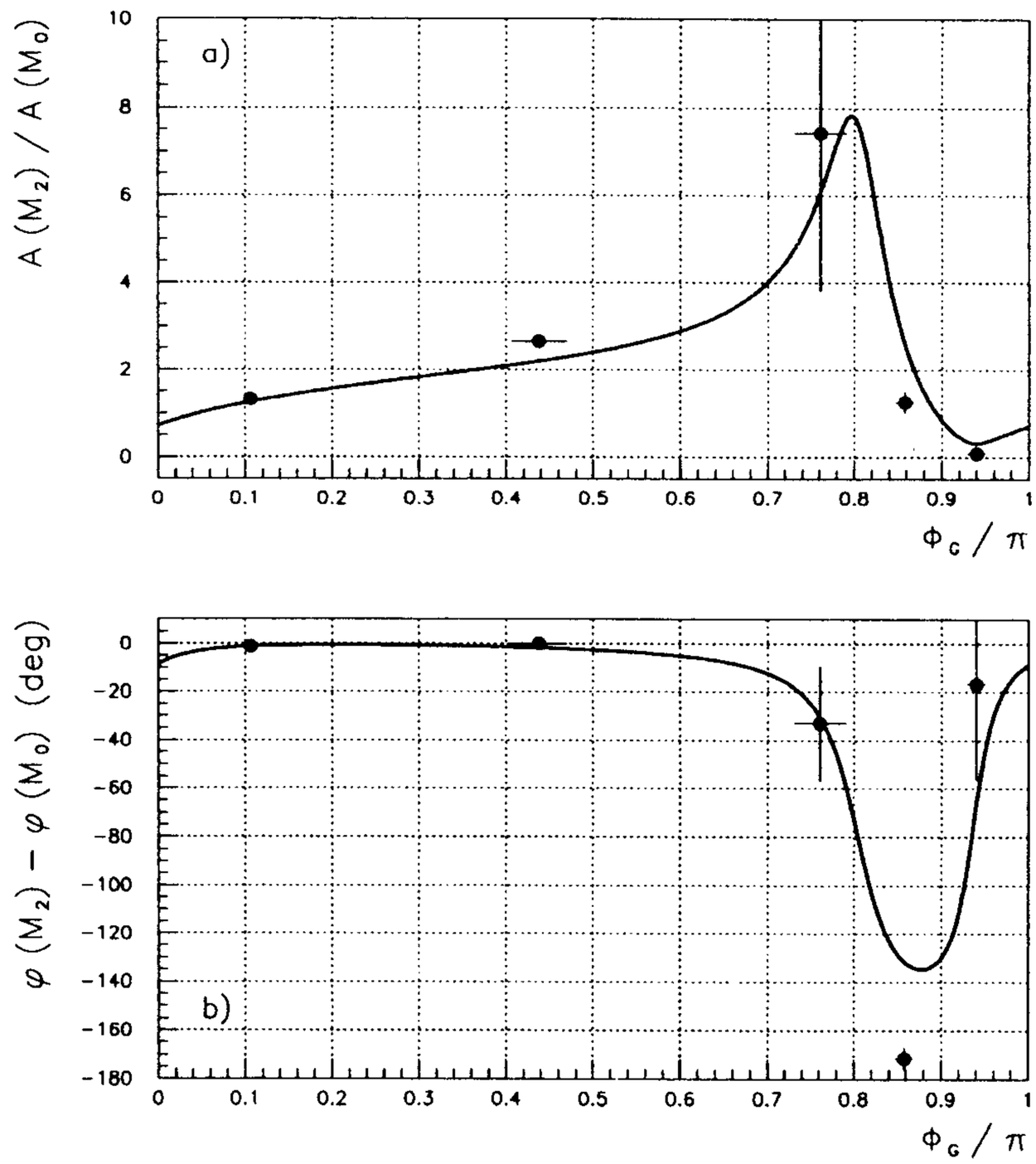

Fig. 3. Comparison between theory and measurements for (a) the ratio $A(M_2)/A(M_0)$ and (b) the phase difference $\varphi(M_2) - \varphi(M_0)$ expressed as a function of the Guoy phase Φ_G.

inserting a lens between it and the output mirror, at whose position we define the zero of the Guoy phase. The quoted errors are only computed from the measured noise fluctuations. In all the cases the agreement appears extremely satisfactory.

The effect of the evolution of the Guoy phase has been directly tested on the beam reflected from M_0. As indicated at the end of Section 2.2, we have kept Q_0 fixed at about 60 cm from M_0, and placed a lens with $f = +20$ cm at different distances from Q_0, thus obtaining values for the total Guoy phase in the range $(0.11–0.94)\pi$ rad. The behaviours of both

$A(M_2)/A(M_0)$ and $\varphi(M_2) - \varphi(M_0)$, expressed in terms of the calculated Guoy phase Φ_G, are shown in Fig. 3.

The expected curve for $A(M_2)/A(M_0)$ peaks quite sharply at $\Phi_G/\pi = 0.8$ and the experimental data follow this shape with a reasonable agreement. The smallness of the $A(M_0)$ value at the peak position makes the error bar on the ratio unusually large. The same observation holds for $\varphi(M_2) - \varphi(M_0)$ as well. By looking at the two figures, one could argue that there is a possible small systematic shift, of approximately 9 degrees, between theory and experiment. While there are a lot of possible explanations for that, one has to keep in mind that the theoretical curves have been computed using the measured values for distances, transmittivities, etc., and thus they can be affected by systematic uncertainties as well.

The validity of this theoretical approach can be further appreciated in the following way. Starting from a coarse pre-alignment condition, one can read the residual error signals given by the three photodiodes and elaborate the corrections to be applied to each individual mirror for the fine alignment of the system. The sequence of the power levels that the dark fringe detector reads, when the corrections are applied one after the other, is presented in Fig. 4. With this correction procedure the light extinction on the dark fringe improves of more than a factor 3, reaching a value of 0.4% of the total power stored into the cavity.

In conclusion, we have demonstrated that even with a very low average power in the photodiodes, (1–30) μW, a small phase modulation index (0.25% of the total power in each sideband) and a longitudinal locking scheme that could be largely improved, it is possible to accurately align a complex interferometer. Indeed, under these circumstances, the average noise level on the demodulated signals from the quadrant photodiodes is equivalent to about 10 nrad/$\sqrt{\text{Hz}}$ or $4.0 \times 10^{-5}\alpha_0/\sqrt{\text{Hz}}$. Therefore, since this angle is the minimum angle that can be detected in our setup, this quoted value represents the lowest limit to our present alignment capability. Finally, since the VIRGO sensitivity to GW detection requires the angular noise to be reduced below 1 μrad/$\sqrt{\text{Hz}}$ [10], we claim that our present results already satisfy this requirement.

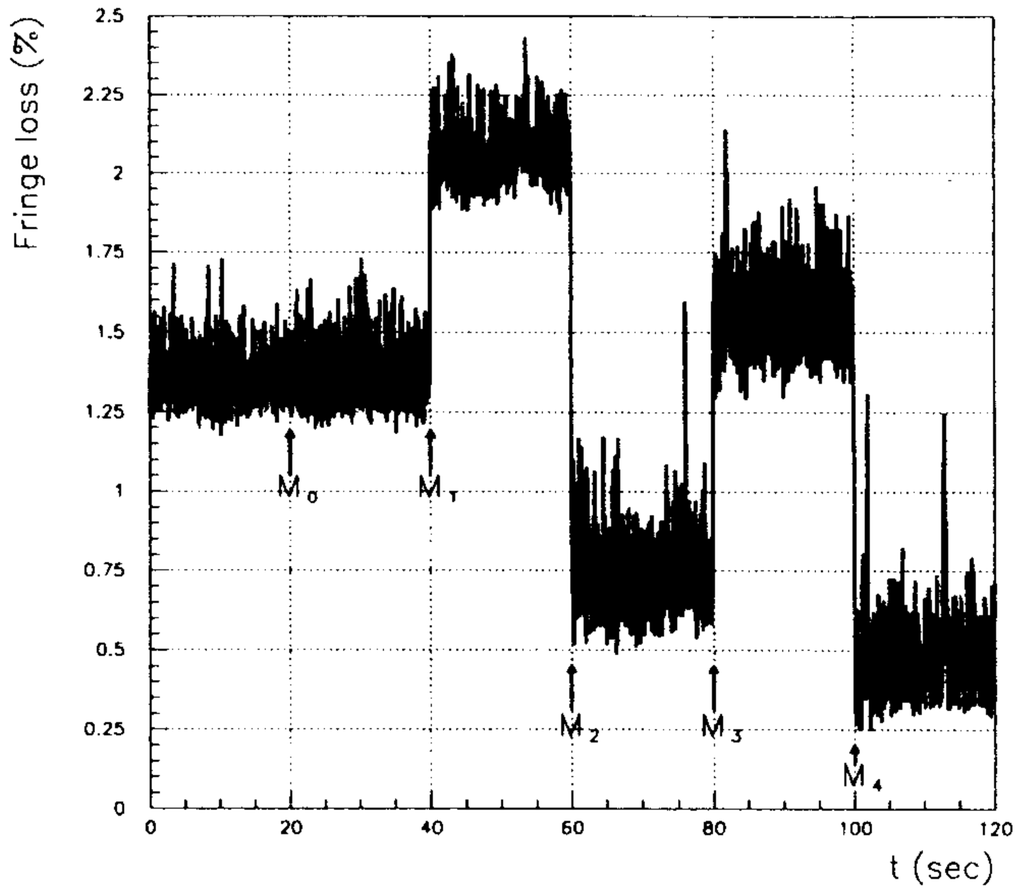

Fig. 4. Fringe loss (the ratio between the power on the fringe detector and the power in the recycling cavity) when the calculated corrections are applied in sequence to $M_{0,1,2,3,4}$.

Acknowledgement

We want to express our appreciation to the VIRGO-Frascati technical team, E. Cima, M. Iannarelli and E. Turri, for their great assistance during the construction and operation of the interferometer.

References

[1] A. Giazotto, First E. Amaldi conference on gravitational wave experiments, Villa Tuscolana, Frascati (Rome), 14–17 June 1994.
[2] A. Abramovici et al., Science 256 (1992) 325.
[3] J. Hough et al., Proposal for a 600 m laser interferometric gravitational antenna – GEO 600, proposal to the PPARC (1994).
[4] D.Z. Anderson, Appl. Opt. 23 (1984) 2944;
N.M. Sampas and D.Z. Anderson, Appl. Opt. 29 (1990) 394.
[5] E. Morrison et al., Appl. Opt. 33 (1994), 5041.
[6] R.W. Drever et al., Appl. Phys. B 31 (1983) 97.
[7] D. Babusci et al., Frascati Internal Report LNF-94/027 (IR).
[8] R. Flaminio and H. Heitman, Phys. Lett. A 214 (1996) 112.
[9] L. Matone, Automatic alignment method for the VIRGO laser interferometer, Master thesis in physics, Rome II University (1996), unpublished [in Italian].
[10] VIRGO Collaboration, Final design (1995).